Appeared in IVC (the Journal of Image and Vision Computing)

Triangulation for Points on Lines

Adrien Bartoli and Jean-Thierry Lapresté
LASMEA – CNRS / Université Blaise Pascal
Clermont-Ferrand, France
Adrien.Bartoli@gmail.com

February 22, 2007

Manuscript Number: IMAVIS-D-06-00159 – First revision
Paper submitted to IVC (Image and Vision Computing). Note: This is an extended version of our ECCV'06 publication (European Conference on Computer Vision, Graz, Austria, May 2006) that can be found on the web:
http://www.lasmea.univ-bpclermont.fr/Personnel/Adrien.Bartoli /Publications/Bartoli_Lapreste_ECCV06.pdf
The main difference is that the submitted version contains new experimental results. Some equations have been expanded and rewritten for clarity, and some figures added. The algebraic method is described in more details.

Abstract

Triangulation consists in finding a 3D point reprojecting the best as possible onto corresponding image points. It is classical to minimize the reprojection error, which, in the pinhole camera model case, is nonlinear in the 3D point coordinates. We study the triangulation of points lying on a 3D line, which is a typical problem for Structure-From-Motion in man-made environments. We show that the reprojection error can be minimized by finding the real roots of a polynomial in a single variable, which degree depends on the number of images. We use a set of transformations in 3D and in the images to make the degree of this polynomial as low as possible, and derive a practical reconstruction algorithm. Experimental comparisons with an algebraic approximation algorithm and minimization of the reprojection error using Gauss-Newton are reported for simulated and real data. Our algorithm finds the optimal solution with high accuracy in all cases, showing that the polynomial equation is very stable. It only computes the roots corresponding to feasible points, and can thus deal with a very large number of views – triangulation from hundreds of views is performed in a few seconds. Reconstruction accuracy is shown to be greatly improved compared to standard triangulation methods that do not take the line constraint into account.

Index Terms: Triangulation, Structure-From-Motion, Point, Line.

1 Introduction

Triangulation is one of the main building blocks of Structure-From-Motion algorithms. Given image feature correspondences and camera matrices, it consists in finding the position of the underlying 3D feature, by minimizing some error criterion. This criterion is often chosen as the reprojection error – the Maximum Likelihood criterion for a Gaussian, centred and *i.i.d.* noise model on the image point positions - though other criteria are possible [5, 9, 10].

Traditionally, triangulation is carried out by some sub-optimal procedure and is then refined by local optimization, see *e.g.* [7]. A drawback of this is that convergence to the optimal solution is not guaranteed. Optimal procedures for triangulating points from two and three views were proposed in [6, 13].

We address the problem of triangulating points lying on a line, that is, given image point correspondences, camera matrices and a 3D line, finding the 3D point lying on the 3D line, such that the reprojection error is minimized.

Our main contribution is to show that the problem can be solved by computing the real roots of a degree-($3n$-2) polynomial, where n is the number of views. Extensive experiments on simulated data show that the polynomial is very well balanced since large number of views and large level of noise are handled. The method is valid whatever the calibration level of the cameras is – projective, affine, metric or Euclidean.

One may argue that triangulating points on a line only has a theoretical interest since in practice, triangulating a line from multiple views is done by minimizing the reprojection error over its supporting points which 3D positions are hence reconstructed along with the 3D line. Indeed, most work consider the case where the supporting points do *not* match accross the images, see *e.g.* [3]. When one identifies correspondences of supporting points accross the images, it is fruitful to incorporate these constraints into the bundle adjustment, as is demonstrated by our experiments. This is typically the case in man-made environments, where one identifies *e.g.* matching corners at the meet of planar facades or around windows. Bartoli *et al.* [2] dubbed Pencil-of-Points or 'POP' this type of features. In order to find an initial 3D reconstruction, a natural way is to compute the 3D line by some means (*e.g.* by ignoring the matching constraints of the supporting points, from 3D primitives such as the intersection of two planes, or from a registered wireframe CAD model) and then to triangulate the supporting point correspondences using point on line triangulation. The result can then be plugged into a bundle adjustment incorporating the constraints.

We review some related work in §2. Our triangulation method is derived in §3. A linear least squares method minimizing an algebraic distance is provided in §4. Gauss-Newton refinement is summarized in §5. Experimental results are reported in §6 and our conclusions in §7.

Notation. Vectors are written using bold fonts, *e.g.* $\mathbf{q}$, and matrices using sans-serif fonts, *e.g.* P. Almost everything is homogeneous, *i.e.* defined up to scale. Equality up to scale is denoted $\sim$. The inhomogenous part of a vector is denoted using a bar, *e.g.* $\mathbf{q}^\mathsf{T} \sim (\bar{\mathbf{q}}^\mathsf{T} \; 1)$ where $^\mathsf{T}$ is transposition. Index $i = 1, \ldots, n$, and sometime j are used for the images. The point in the i-th image is $\mathbf{q}_i$. Its elements are $\mathbf{q}_i^\mathsf{T} \sim (q_{i,1} \;\; q_{i,2} \;\; 1)$. The 3D line joining points $\mathbf{M}$ and $\mathbf{N}$ is denoted $(\mathbf{M}, \mathbf{N})$. The $\mathcal{L}_2$-norm of a vector is denoted as in $\|\mathbf{x}\|^2 = \mathbf{x}^\mathsf{T}\mathbf{x}$. The Euclidean distance measure d_e is defined by:

$$d_e^2(\mathbf{x}, \mathbf{y}) = \left\| \frac{\mathbf{x}}{x_3} - \frac{\mathbf{y}}{y_3} \right\|^2 = \left(\frac{x_1}{x_3} - \frac{y_1}{y_3} \right)^2 + \left(\frac{x_2}{x_3} - \frac{y_2}{y_3} \right)^2. \tag{1}$$

2 Related Work

Optimal procedures for triangulating points in 3D space, and points lying on a plane were previously studied, as summarized in table 1. Hartley and Sturm [6] showed that triangulating points in 3D space from two views, in other words finding a pair of points satisfying the epipolar geometry and lying as close as possible to the measured points, can be solved by finding the real roots of a degree-6 polynomial. The optimal solution is then selected by straightforward evaluation of the reprojection error. Stewénius *et al.* [13] extended the method to three views. The optimal solution is one of the real roots of a system of 3 degree-6 polynomials in the 3 coordinates of the point. Chum *et al.* [4] show that triangulating points lying on a plane, in other words finding a pair of points satisfying an homography and lying as close as possible to the measured points, can be solved by finding the real roots of a degree-8 polynomial.

Type of triangulation	Number of views	Polynomial system			Reference
		Number	Degree	Variables	
Point in 3D space	2	1	6	1	[6]
	3	3	6/6/6	3	[13]
Point on plane	2	1	8	1	[4]
Point on line	1	1	1	1	This paper
	2	1	4	1	
	3	1	7	1	
	4	1	10	1	
	n	1	$3n-2$	1	

Table 1: Different types of triangulation and methods minimizing the $\mathcal{L}_2$-norm reprojection error. The number of polynomials to be solved, their degrees and the number of variables is given in the column 'Polynomial system'.

Error functions different from the reprojection error were considered in the literature. The directional error in two views is proposed in [10], along with a triangulation method for calibrated cameras. The $\mathcal{L}_\infty$-norm is considered in [5, 9], instead of the usual $\mathcal{L}_2$-norm. A triangulation method for two views is given in [9], while it is shown in [5] that the n-view case can be cast as a convex optimization problem.

3 Minimizing the Reprojection Error

We derive our optimal triangulation algorithm for point on line, dubbed 'POLY'.

3.1 Problem Statement and Parameterization

We want to compute a 3D point $\mathbf{Q}$, lying on a 3D line $(\mathbf{M}, \mathbf{N})$, represented by two 3D points $\mathbf{M}$ and $\mathbf{N}$. The (3×4) perspective camera matrices are denoted P_i with $i = 1, \ldots, n$ the image index. The problem is to find the point $\hat{\mathbf{Q}}$ such that:

$$\hat{\mathbf{Q}} \quad \sim \quad \arg \min_{\mathbf{Q} \in (\mathbf{M}, \mathbf{N})} \mathcal{C}_n^2(\mathbf{Q}),$$

where $\mathcal{C}_n$ is the n-view *reprojection error*:

$$\mathcal{C}_n^2(\mathbf{Q}) \quad = \quad \sum_{i=1}^{n} d_e^2(\mathbf{q}_i, \mathsf{P}_i \mathbf{Q}). \tag{2}$$

We parameterize the point $\mathbf{Q} \in (\mathbf{M}, \mathbf{N})$ using a single parameter $\lambda \in \mathbb{R}$ as:

$$\mathbf{Q} \sim \lambda \mathbf{M} + (1 - \lambda) \mathbf{N} \sim \lambda(\mathbf{M} - \mathbf{N}) + \mathbf{N}. \tag{3}$$

Introducing this parameterization into the reprojection error (2) yields:

$$\mathcal{C}_n^2(\lambda) \quad = \quad \sum_{i=1}^{n} d_e^2(\mathbf{q}_i, \mathsf{P}_i(\lambda(\mathbf{M} - \mathbf{N}) + \mathbf{N})).$$

Defining $\mathbf{b}_i = \mathsf{P}_i(\mathbf{M} - \mathbf{N})$ and $\mathbf{d}_i = \mathsf{P}_i \mathbf{N}$, we get:

$$\mathcal{C}_n^2(\lambda) \quad = \quad \sum_{i=1}^{n} d_e^2(\mathbf{q}_i, \lambda \mathbf{b}_i + \mathbf{d}_i). \tag{4}$$

Note that a similar parameterization can be derived by considering the inter-image homographies induced by the 3D line [12]. The main motivation to reducing the number of parameters with parameterization (3) instead of using, *e.g.* a Lagrange multiplier for the point on line constraint, is that it allows us to find the global minimum of the reprojection error through a simple polynomial formulation.

3.2 Simplification

We simplify the expression (4) of the reprojection error by changing the 3D coordinate frame and the image coordinate frames. This is intended to lower the degree of the polynomial equation that will ultimately have to be solved. Since the reprojection error is based on Euclidean distances measured in the images, only rigid image transformations are allowed to keep invariant the error function, while full projective homographies can be used in 3D. We thus setup a standard canonical 3D coordinate frame, see *e.g.* [8], such that the first camera matrix becomes $\mathsf{P}_1 \sim (\ \mathrm{I} \quad \mathbf{0})$. Note that using a projective basis does not harm Euclidean triangulation since the normalization is undone once the point is triangulated. The canonical basis is setup by the following simple operations:

$$\mathsf{H} \leftarrow \begin{pmatrix} & \mathsf{P}_1 & & \\ 0 & 0 & 0 & 1 \end{pmatrix} \qquad \mathsf{P}_i \leftarrow \mathsf{P}_i \mathsf{H}^{-1} \qquad \mathbf{M} \leftarrow \mathsf{H}\mathbf{M} \qquad \mathbf{N} \leftarrow \mathsf{H}\mathbf{N}.$$

Within this coordinate frame, we can write $\mathbf{M}^\mathsf{T} = (\bullet \;\; \bullet \;\; 1 \;\; \bullet)$ and $\mathbf{N}^\mathsf{T} = (\bullet \;\; \bullet \;\; 1 \;\; \bullet)$ without loss of generality, as pointed out in [7, §A6], from which we get:

$$\begin{aligned} \mathbf{b}_1 &= \mathsf{P}_1(\mathbf{M} - \mathbf{N}) = (b_{1,1} \;\; b_{1,2} \;\; 0)^\mathsf{T} \\ \mathbf{d}_1 &= \mathsf{P}_1\mathbf{N} = (d_{1,1} \;\; d_{1,2} \;\; 1)^\mathsf{T}. \end{aligned}$$

We then apply a rigid transformation T_i in each image defined such that $\mathsf{T}_i\mathbf{b}_i$ lies on the y-axis and such that $\mathsf{T}_i\mathbf{d}_i = \mathsf{T}_i\mathsf{P}_i\mathbf{N}$ lies at the origin. This requires that point $\mathbf{N}$ does not project at infinity in any of the images. We ensure this by constraining $\mathbf{N}$ to project as close as possible to one of the image points[1], say $\mathbf{q}_1$. The reprojection error (4) for the first view is $\mathcal{C}_1^2(\lambda) = d_e^2(\mathbf{q}_1, \lambda\mathbf{b}_1 + \mathbf{d}_1) = \|\lambda\bar{\mathbf{b}}_1 + \bar{\mathbf{d}}_1 - \bar{\mathbf{q}}_1\|^2$. We compute λ as the solution of $\frac{\partial \mathcal{C}_1^2}{\partial \lambda} = 0$, which gives, after some minor calculations, $\lambda = (\bar{\mathbf{q}}_1 - \bar{\mathbf{d}}_1)^\mathsf{T}\bar{\mathbf{b}}_1 / \|\bar{\mathbf{b}}_1\|^2$. Substituting in equation (3) yields the following operations:

$$\mathbf{N} \quad \leftarrow \quad \frac{(\mathsf{P}_1\mathbf{N} - \mathbf{q}_1)^\mathsf{T}\mathsf{P}_1(\mathbf{M} - \mathbf{N})}{\|\mathsf{P}_1(\mathbf{M} - \mathbf{N})\|^2}(\mathbf{M} - \mathbf{N}) + \mathbf{N}.$$

Obviously, the $\mathbf{d}_i = \mathsf{P}_i\mathbf{N}$ must be recomputed. These simplications lead to:

$$\begin{cases} \mathbf{b}_1 &= (0 \;\; b_{1,2} \;\; 0)^\mathsf{T} \\ \mathbf{d}_1 &= (0 \;\; 0 \;\; 1)^\mathsf{T} \\ \mathbf{b}_{i>1} &= (0 \;\; b_{i,2} \;\; b_{i,3})^\mathsf{T} \\ \mathbf{d}_{i>1} &= (0 \;\; 0 \;\; d_{i,3})^\mathsf{T}. \end{cases}$$

The rigid transformations T_i are quickly derived below. For each image i, we look for T_i mapping $\mathbf{d}_i$ to the origin, and $\mathbf{b}_i$ to a point on the y-axis. We decompose T_i as a rotation around the origin and a translation:

$$\mathsf{T}_i \quad = \quad \begin{pmatrix} \mathsf{R}_i & \mathbf{0} \\ \mathbf{0}^\mathsf{T} & 1 \end{pmatrix} \begin{pmatrix} \mathrm{I} & -\mathbf{t}_i \\ \mathbf{0}^\mathsf{T} & 1 \end{pmatrix}.$$

The translation is directly given from $\mathsf{T}_i\mathbf{d}_i \sim (0 \;\; 0 \;\; 1)^\mathsf{T}$ as $\mathbf{t}_i = \bar{\mathbf{d}}_i / d_{i,3}$. For the rotation, we consider $\mathsf{T}_i\mathbf{b}_i \sim (0 \;\; \bullet \;\; \bullet)^\mathsf{T}$, from which, setting $\mathbf{r}_i = \bar{\mathbf{b}}_i - b_{i,3}\mathbf{t}_i$, we obtain $\mathsf{R}_i = \begin{pmatrix} r_{i,2} & -r_{i,1} \\ r_{i,1} & r_{i,2} \end{pmatrix} / \|\bar{\mathbf{r}}_i\|$.

[1] Note that this is equivalent to solving the single view triangulation problem. Point $\mathbf{N}$ does not project at infinity in any of the views since both point $\mathbf{q}_1$ and the supporting line have observable correspondences in all images.

This leads to the following expression for the reprojection error (4) where we separated the leading term:

$$\begin{aligned}\mathcal{C}_n^2(\lambda) &= d_e^2(\mathbf{q}_1, \lambda\mathbf{b}_1 + \mathbf{d}_1) + \sum_{i=2}^{n} d_e^2(\mathbf{q}_i, \lambda\mathbf{b}_i + \mathbf{d}_i) \\ &= q_{1,1}^2 + (\lambda b_{1,2} - q_{1,2})^2 + \sum_{i=2}^{n}\left(q_{i,1}^2 + \left(\frac{\lambda b_{i,2}}{\lambda b_{i,3} - d_{i,3}} - q_{i,2}\right)^2\right).\end{aligned}$$

The constant terms $q_{1,1}^2$ and $q_{i,1}^2$ represent the vertical counterparts of the point to line distance in the images. This means that only the errors along the lines are to be minimized.

<u>Objective</u>

Given a point correspondence $\mathbf{q}_i$ over $n \geq 1$ views ($i = 1, \ldots, n$), a 3D line $(\mathbf{M}, \mathbf{N})$ and camera matrices P_i, compute the 3D point $\hat{\mathbf{Q}}$ lying on $(\mathbf{M}, \mathbf{N})$ such that the reprojection error e in all images is minimized.

<u>Algorithm</u>

- **Canonical 3D coordinate frame.** Express the 3D line and the cameras in a canonical 3D coordinate frame:

$$\mathsf{H} \leftarrow \begin{pmatrix} & \mathsf{P}_1 & & \\ 0 & 0 & 0 & 1 \end{pmatrix} \qquad \mathsf{P}_i \leftarrow \mathsf{P}_i\mathsf{H}^{-1} \qquad \mathbf{M} \leftarrow \mathsf{H}\mathbf{M} \qquad \mathbf{N} \leftarrow \mathsf{H}\mathbf{N}$$

  Normalize the homogeneous coordinates: $\mathbf{M} \leftarrow \mathbf{M}/M_3$ and $\mathbf{N} \leftarrow \mathbf{N}/N_3$.

- **Line reparameterization.** Reparameterize the 3D line by shifting point $\mathbf{N}$ such that it projects to a finite point in every views:

$$\mathbf{N} \quad \leftarrow \quad \frac{(\mathsf{P}_1\mathbf{N} - \mathbf{q}_1)^\mathsf{T}\mathsf{P}_1(\mathbf{M} - \mathbf{N})}{\|\mathsf{P}_1(\mathbf{M} - \mathbf{N})\|^2}(\mathbf{M} - \mathbf{N}) + \mathbf{N}$$

  Project the 3D line onto the images: $\mathbf{b}_i \leftarrow \mathsf{P}_i(\mathbf{M} - \mathbf{N})$ and $\mathbf{d}_i \leftarrow \mathsf{P}_i\mathbf{N}$.

- **Rigid image transformations.** Align the projected line with the y-axis in each view such that point $\mathbf{N}$ projects to the origin:

$$\mathbf{t}_i \leftarrow \bar{\mathbf{d}}_i/d_{i,3} \qquad \mathbf{r}_i \leftarrow \bar{\mathbf{b}}_i - b_{i,3}\mathbf{t}_i \qquad \mathsf{R}_i \leftarrow \begin{pmatrix} r_{i,2} & -r_{i,1} \\ r_{i,1} & r_{i,2} \end{pmatrix} / \|\bar{\mathbf{r}}_i\| \qquad \mathsf{T}_i \leftarrow \begin{pmatrix} \mathsf{R}_i & -\mathsf{R}_i\mathbf{t}_i \\ \mathbf{0}^\mathsf{T} & 1 \end{pmatrix}$$

$$\mathbf{d}_i \leftarrow \mathsf{T}_i\mathbf{d}_i \qquad \mathbf{b}_i \leftarrow \mathsf{T}_i\mathbf{b}_i \qquad \mathsf{P}_i \leftarrow \mathsf{T}_i\mathsf{P}_i \qquad \mathbf{q}_i \leftarrow \mathsf{T}_i\mathbf{q}_i$$

- **Solving.** See §3.3 for how to find the real roots λ_k of the polynomial $\tilde{\mathcal{D}}(\lambda)$ given by equation (5). Select the root $\hat{\lambda}$ for which the reprojection error is minimized: $\hat{\lambda} = \arg\min_k \mathcal{C}_n^2(\lambda_k)$.

- **Finishing.** Compute the mean reprojection error $e = \sqrt{\frac{1}{n}\mathcal{C}_n^2\left(\hat{\lambda}\right)}$ and recover the 3D point in the original coordinate frame: $\hat{\mathbf{Q}} \sim \mathsf{H}^{-1}\left(\hat{\lambda}\mathbf{M} + \left(1 - \hat{\lambda}\right)\mathbf{N}\right)$.

Table 2: The proposed point on line triangulation algorithm 'Poly'.

3.3 Solving the Polynomial Equation

Looking for the minima of the reprojection error $\mathcal{C}_n^2$ is equivalent to finding the roots of its derivative, *i.e.* solving $\frac{\partial \mathcal{C}_n^2}{\partial \lambda} = 0$. Define $\mathcal{D}_n = \frac{1}{2}\frac{\partial \mathcal{C}^2}{\partial \lambda}$:

$$\mathcal{D}_n(\lambda) = (\lambda b_{1,2} - q_{1,2})b_{1,2} + \sum_{i=2}^{n} \left(\frac{\lambda b_{i,2}}{\lambda b_{i,3} + d_{i,3}} - q_{i,2} \right) \left(\frac{b_{i,2} d_{i,3}}{(\lambda b_{i,3} + d_{i,3})^2} \right).$$

This is a nonlinear function. Directly solving $\mathcal{D}_n(\lambda) = 0$ is therefore very difficult in general. We thus define $\tilde{\mathcal{D}}_n(\lambda) = \mathcal{D}_n(\lambda)\mathcal{K}_n(\lambda)$, where we choose $\mathcal{K}_n$ in order to cancel out the denominators including λ in $\mathcal{D}_n$. Finding the zeros of $\tilde{\mathcal{D}}_n$ is thus equivalent to finding the zeros of $\mathcal{D}_n$. Inspecting the expression of $\mathcal{D}_n$ reveals that $\mathcal{K}_n(\lambda) = \prod_{i=2}^{n} (\lambda b_{i,3} + d_{i,3})^3$ does the trick:

$$\begin{aligned} \tilde{\mathcal{D}}_n(\lambda) = (\lambda b_{1,2} - q_{1,2}) b_{1,2} \prod_{i=2}^{n} (\lambda b_{i,3} + d_{i,3})^3 \\ + \sum_{i=2}^{n} \left(b_{i,2} d_{i,3} \left(\lambda b_{i,2} - q_{i,2}(\lambda b_{i,3} + d_{i,3}) \right) \prod_{j=2, j \neq i}^{n} (\lambda b_{j,3} + d_{j,3})^3 \right). \end{aligned} \tag{5}$$

As expected, $\tilde{\mathcal{D}}_n$ is a polynomial function, whose degree depends on the number of images n. We observe that cancelling the denominator out for the contribution of each $(i > 1)$-image requires to multiply $\mathcal{D}_n$ by a cubic, namely $(\lambda b_{i,3} + d_{i,3})^3$. Since the polynomial required for image $i = 1$ is linear, the degree of the polynomial to solve is $3(n-1) + 1 = 3n - 2$.

Given the real roots λ_k of $\tilde{\mathcal{D}}_n(\lambda)$, that we compute as detailed below for different number of images, we simply select the one for which the reprojection error is minimized, *i.e.* $\hat{\lambda} = \arg\min_k \mathcal{C}_n^2(\lambda_k)$, substitute it in equation (3) and transfer the recovered point back to the original coordinate frame:

$$\hat{\mathbf{Q}} \sim \mathsf{H}^{-1} \left(\hat{\lambda} \mathbf{M} + \left(1 - \hat{\lambda} \right) \mathbf{N} \right).$$

A single image. For $n = 1$ image, the point is triangulated by projecting its image onto the image projection of the line. The intersection of the associated viewing ray with the 3D line gives the 3D point. In our framework, equation (5) is indeed linear in λ for $n = 1$:

$$\tilde{\mathcal{D}}_1(\lambda) \quad = \quad (\lambda b_{1,2} - q_{1,2}) b_{1,2} = b_{1,2}^2 \lambda - q_{1,2} b_{1,2}.$$

A pair of images. For $n = 2$ images, equation (5) gives:

$$\tilde{\mathcal{D}}_2(\lambda) = (\lambda b_{1,2} - q_{1,2}) b_{1,2} (\lambda b_{2,3} + d_{2,3})^3 + b_{2,2} d_{2,3} (\lambda b_{2,2} - q_{2,2}(\lambda b_{2,3} + d_{2,3})),$$

which is a quartic in λ that can be solved in closed-form using Cardano's formulas: $\tilde{\mathcal{D}}_2(\lambda) \sim \sum_{d=1}^{4} c_d \lambda^d$, with:

$$\left\{ \begin{array}{lcl} c_0 & = & -q_{2,2}d_{2,3}^2 b_{2,2} - b_{1,2}q_{1,2}d_{2,3}^3 \\ c_1 & = & d_{2,3}(b_{2,2}^2 - 3b_{1,2}q_{1,2}b_{2,3}d_{2,3} + b_{1,2}^2 d_{2,3}^2 - q_{2,2}b_{2,3}b_{2,2}) \\ c_2 & = & 3b_{1,2}b_{2,3}d_{2,3}(b_{1,2}d_{2,3} - q_{1,2}b_{2,3}) \\ c_3 & = & b_{1,2}b_{2,3}^2(3b_{1,2}d_{2,3} - q_{1,2}b_{2,3}) \\ c_4 & = & b_{1,2}^2 b_{2,3}^3. \end{array} \right.$$

Multiple images. Solving the $n \geq 3$ view case is done in two steps. The first step is to compute the coefficients c_j, $j = 0, \ldots, 3n$-2 of a polynomial. The second step is to compute its real roots. Computing the coefficients in closed-form from equation (5), as is done above for the single- and the two-view cases, lead to very large, awkward formulas, which may lead to roundoff errors. We thus perform a numerical computation, while reparameterizing the polynomial, as described below.

A standard root-finding technique is to compute the eigenvalues of the ((3n-2)$\times$(3n-2)) companion matrix of the polynomial, see *e.g.* [1]. Computing all the roots ensures the optimal solution to be found. This can be done if the number of images is not too large, *i.e.* lower than 100, and if computation time is not an issue. However, for large numbers of images, or if real-time computation must be achieved, it is not possible to compute and try all roots. In that case, we propose to compute only the roots corresponding to feasible points.

Let λ_0 be an approximation of the sought-after root. For example, one can take the result of the algebraic method of §4, or even $\lambda_0 = 0$ since our parameterization takes the sought-after root very close to 0. Obviously, we could launch an iterative root-finding procedure such as Newton-Raphson from λ_0 but this would not guarantee that the optimal solution is found.

One solution to efficiently compute only the feasible roots is to reparameterize the polynomial such that those lie close to 0, and use an iterative algorithm for computing the eigenvalues of the companion matrix on turn. For example, Arnoldi or Lanczos' methods, compute the eigenvalues with increasing magnitude starting from the smallest one. Let λ_c be the last computed eigenvalue, and $\mathbf{Q}_1$ and $\mathbf{Q}_2$ the reconstructed points corresponding to λ_c and $-\lambda_c$. If both $\mathbf{Q}_1$ and $\mathbf{Q}_2$ reproject outside the images, the computation is stopped. Indeed, the next root that would be computed would have greater magnitude than λ_c, and would obviously lead to a point reprojecting further away than the previous one outside the images.

The reparameterization is done by computing a polynomial $\mathcal{P}_n(\lambda) = \tilde{\mathcal{D}}_n(\lambda + \lambda_0)$. A simple way to achieve this reparameterization is to estimate the coefficients c_j, $j = 1, \ldots, 3n$-1, of $\mathcal{P}_n$, as follows. We evaluate $z \geq 3n$-1 values $v_k = \tilde{\mathcal{D}}_n(\lambda_k + \lambda_0)$ from equation (5) for $\lambda_k \in [-\delta, \delta]$, and solve the associated Vandermonde system:

$$\sum_{j=0}^{3n-2} c_j \lambda_k^j \quad = \quad v_k \quad \text{for } k = 1, \ldots, z.$$

We typically use $z = 10(3n\text{-}1)$. The parameter $\delta \in \mathbb{R}^{*+}$ reflects the size of the sampling interval around λ_0. We noticed that this parameter does not influence the results, and typically chose $\delta = 1$. Obviously, in theory, using $z = 3n\text{-}1$, *i.e.* the minimum number of samples, at distinct points, is equivalent for finding the coefficients. However we experimentally found that using extra samples evenly spread around the expected root λ_0 has the benefit of 'averaging' the roundoff error, and stabilizes the computation.

One could argue that with this method for estimating the coefficients, the simplifying transformations of §3.2 are not necessary. A short calculation shows that this is partly true since if the canonical 3D projective basis were not used along with the normalization of the third entries of $\mathbf{M}$ and $\mathbf{N}$ to unity, then the degree of the polynomial would be $3n$ instead of $3n\text{-}2$. While this makes little difference for large n, this is important *e.g.* for finding a closed-form solution in the two-view case. Such low n cases are likely to be embedded in RANSAC schemes, making triangulation time critical.

4 An Algebraic Criterion

We give a linear algorithm, dubbed 'Algebraic', based on approximating the reprojection error (2) by replacing the Euclidean distance measure d_e by the algebraic distance measure d_a defined by $d_a^2(\mathbf{x}, \mathbf{y}) = \mathsf{S}[\mathbf{x}]_\times \mathbf{y}$ with $\mathsf{S} = \left(\begin{smallmatrix} 1 & 0 & 0 \\ 0 & 1 & 0 \end{smallmatrix}\right)$, and:

$$d_a^2(\mathbf{x}, \mathbf{y}) \quad = \quad \mathsf{S}[\mathbf{x}]_\times \mathbf{y} \qquad \text{with} \qquad \mathsf{S}_{(2\times 3)} = \begin{pmatrix} 1 & 0 & 0 \\ 0 & 1 & 0 \end{pmatrix},$$

where $[\mathbf{x}]_\times$ is the (3×3) skew-symmetric matrix associated to cross-product, *i.e.* $[\mathbf{x}]_\times \mathbf{y} = \mathbf{x} \times \mathbf{y}$. This gives an algebraic error function:

$$\mathcal{E}_n^2(\lambda) = \sum_{i=1}^{n} d_a^2(\lambda \mathbf{b}_i + \mathbf{d}_i, \mathbf{q}_i) = \sum_{i=1}^{n} \|\lambda \mathsf{S}[\mathbf{q}_i]_\times \mathbf{b}_i + \mathsf{S}[\mathbf{q}_i]_\times \mathbf{d}_i\|^2,$$

in matrix form:

$$\mathcal{E}_n^2(\lambda) \quad = \quad \left\| \begin{pmatrix} \cdots \\ \mathsf{S}[\mathbf{q}_i]_\times \mathbf{b}_i \\ \cdots \end{pmatrix}_{(2n\times 1)} \lambda + \begin{pmatrix} \cdots \\ \mathsf{S}[\mathbf{q}_i]_\times \mathbf{d}_i \\ \cdots \end{pmatrix}_{(2n\times 1)} \right\|^2.$$

A closed-form solution is obtained, giving λ_a in the least squares sense:

$$\lambda_a \quad = \quad -\frac{\sum_{i=1}^n \mathbf{b}_i^\mathsf{T} [\mathbf{q}_i]_\times \tilde{\mathrm{I}} [\mathbf{q}_i]_\times \mathbf{d}_i}{\sum_{i=1}^n \mathbf{b}_i^\mathsf{T} [\mathbf{q}_i]_\times \tilde{\mathrm{I}} [\mathbf{q}_i]_\times \mathbf{b}_i} \qquad \text{with} \qquad \tilde{\mathrm{I}} \sim \mathsf{S}^\mathsf{T}\mathsf{S} \sim \left(\begin{smallmatrix} 1 & 0 & 0 \\ 0 & 1 & 0 \\ 0 & 0 & 0 \end{smallmatrix}\right).$$

Algorithms based on algebraic distances are highly conditioned by the image coordinate frame, see *e.g.* [7]. We experimentally tried the classical normalization used in *e.g.* the eight-point algorithm in [7], and did not notice any difference with the normalization proposed in §3.2 for the polynomial algorithm.

5 Gauss-Newton Refinement

As is usual for triangulation and bundle adjustment [7], we use the Gauss-Newton algorithm for refining an estimate of $\hat{\lambda}$ by minimizing the nonlinear least squares reprojection error (2). The algorithm, that we do not derived in details, is dubbed 'Gauss-Newton'. We use the best solution amongst Poly and Algebraic as the initial solution.

6 Experimental Results

6.1 Simulated Data

We simulated a 3D line observed by n cameras P_i. In order to simulate realistic data, we reconstructed the 3D line as follows. We projected the line onto the images, and regularly sampled points on it, that were offset orthogonally to the image line with a Gaussian centred noise with variance σ_l. The 3D line was then reconstructed from the noisy points using the Maximum Likelihood triangulation method in [3], which provided[2] $\mathbf{M}$ and $\mathbf{N}$. Note that any line triangulation method, see *e.g.* [14], can be used. Finally, a point lying on the true 3D line was projected onto the images, and corrupted with a Gaussian centred noise with variance σ_p, which gave the $\mathbf{q}_i$. We varied some parameters of this setup, namely n and σ_p, and the spatial configuration of the cameras, in order to compare the algorithms under different conditions. We compared two cases for the cameras: a stable one, in which they were evenly spread around the 3D line, and an unstable one, in which they were very close to each other. The default parameters of the setup are $\sigma_l = 0.1$ pixels, $\sigma_p = 3$ pixels, $n = 10$ views and stable cameras.

We had two main goals in these experiments. First, we wanted to determine what in practice is the maximum number of views and noise that the proposed triangulation method can deal with, for stable and unstable camera configurations. Second, we wanted to determine to which extent the line constraint improves the accuracy of the reconstructed 3D point, compared to standard unconstrained triangulation. We measured two kinds of error: the reprojection error, quantifying the ability of the methods to fit the measurements, and a 3D error, quantifying the accuracy of the reconstruction.

We compared the three algorithms, described in the paper (Poly, §3 ; Algebraic, §4 ; Gauss-Newton, §5) and 3DTriangulation, which is a standard Maximum Likelihood triangulation, ignoring the line constraint, *e.g.* [7].

Figure 1 shows the results for varying noise level on the image points ($\sigma_p = 1, \ldots, 10$ pixels), and figure 2 for varying number of views ($n = 2, \ldots, 200$). Note the logarithmic scaling on the abscissa. General comments can be made about these results:

[2] The line triangulation method in [3] provides the Plücker coordinates of the 3D line. Points $\mathbf{M}$ and $\mathbf{N}$ are extracted as the two singular vectors associated to the two non-zero singular values of the rank-two Plücker matrix using SVD. Note that the position of $\mathbf{M}$ and $\mathbf{N}$ along the line does not change the result.

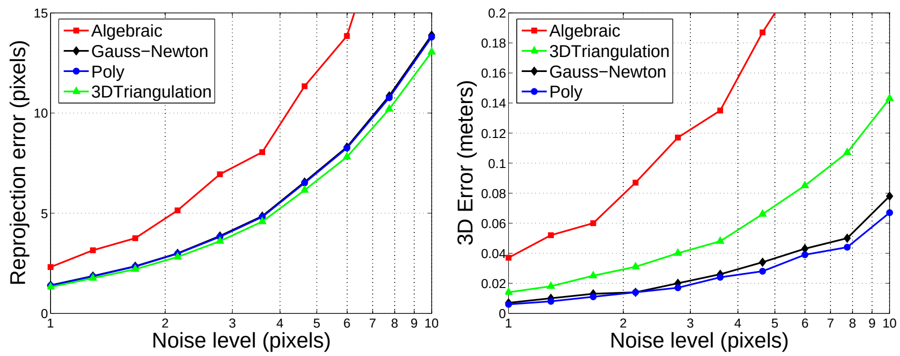

Figure 1: Reprojection error (left) and 3D error (right) versus the level of noise.

- 3DTriangulation always gives the lowest reprojection error.
- Algebraic always gives the highest reprojection error and 3D error.
- Poly and Gauss-Newton always give the lowest 3D error.

Small differences in the reprojection error may lead to large discrepancies in the 3D error. For example, Poly and Gauss-Newton are undistinguisable on figures 1 (left) and 2 (left), showing the reprojection error, while they can clearly be distinguished on figures 1 (right) and 2 (right), showing the 3D error. This is due to the fact that Gauss-Newton converges when some standard precision is reached on the reprojection error. Increasing the precision may improve the results, but would make convergence slower.

For $n = 10$ views, figure 1 shows that the accuracy of the 3D reconstruction is clearly better for the optimal methods Poly and Gauss-Newton using the line constraint, compared to 3DTriangulation that does not use this constraint. The difference in 3D accuracy is getting larger as the noise level increases. For a $\sigma_p = 1$ pixel noise, which is what one can expect in practice, the difference in accuracy is 1 cm, corresponding to 1% of the simulated scene scale. This is an important difference.

However, for $\sigma_p = 3$ pixels, beyond 20 views, figure 2 (left) shows that the reprojection error for 3DTriangulation and Poly/Gauss-Newton are hardly distinguishable, while we expect from figure 2 (right) the difference in 3D error to be negligible beyond 200 views.

The results presented above concern the stable camera setup. For the unstable case, we obtained slightly lower reprojection errors, which is due to the fact that the 3D model is less constrained, making the observations easier to "explain". However, as was expected, the 3D errors are higher by a factor of around 2. The order of the different methods remains the same as in the stable case. We noticed that incorporating the line constraint improves the accuracy compared to 3DTriangulation to a much higher extent than in the stable case.

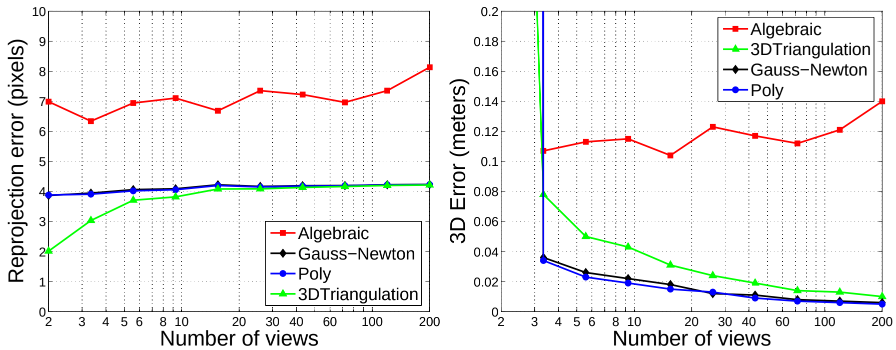

Figure 2: Reprojection error (left) and 3D error (right) versus the number of views.

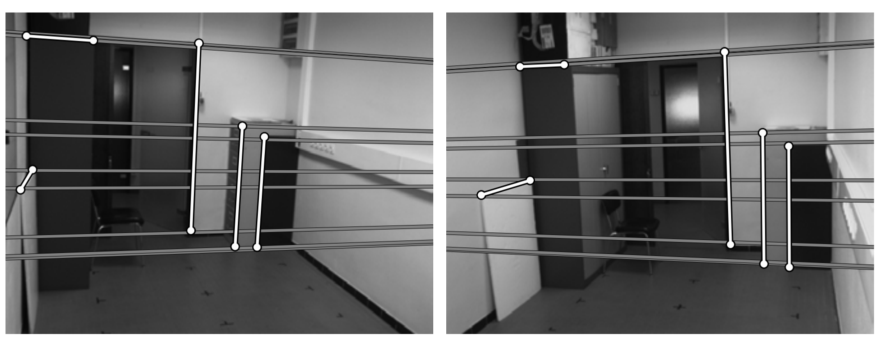

Figure 3: The two original images of the ‘office’ sequence, overlaid with 5 matching segments, 10 corresponding end-points (in white), and their epipolar lines (in gray).

6.2 Real Data

We tested the four reconstruction algorithms on several real data sets. For three of them, we show results. We used a Canny detector to retrieve salient edgels in the images, and adjusted segments using robust least squares. Finally, we matched the segments by hand between the images, except for the 387 frame 'building' sequence where automatic traking was used. The point on line correspondences were manually given, again besides for the 'building' sequence for which correlation based tracking was used. We reconstructed the 3D lines from the edgels by the Maximum Likelihood method in [3].

The 'office' sequence. This data set consists of two images of an indoor scene, shown overlaid with 5 input segments and 10 input points on figure 3. A standard nonlinear least squares algorithm was used to recover the fundamental matrix, from which we extracted a pair of uncalibrated projection matrices. Note that for two views, line triangulation is an exact process. The end-points of matching segments correspond to the same physical point. We thus use them as input to our algorithms. A calibration grid was used to get the radial distortion parameters, that was corrected.

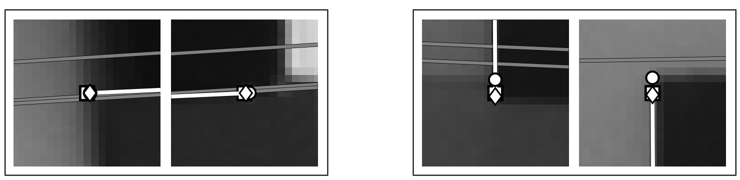

Figure 4: Close up on some reprojected features, around the two end-points for the segment in the left hand corner of figure 3 (left) and in the right most part (right). The epipolar lines are shown in gray, and the segments in white, with their end-points plotted with squares. The diamonds are the points predicted from method Algebraic, and the circles from methods Poly and Gauss-Newton (they are undistinguishable).

This data set is interesting in particular for the reason that one of the segments almost lies on the epipolar lines associated to its end-points, which is one case where line triangulation is singular. Indeed, any 3D line lying on the epipolar plane reprojects to the same image lines. For this segment, we used the fact that the end-points are corresponding, and can thus be triangulated on their own using standard unconstrained triangulation, to disambiguate the 3D line.

Algebraic and Poly/Gauss-Newton gave respectively a 3.45 pixels and a 1.42 pixels reprojection error[3], while 3DTriangulation achieved 0.98 pixels. A close up on the reprojected points can be seen on figure 4.

[3]These are RMS (Root Mean of Squares) errors over all images and all points.

The 'Valbonne church' sequence. We used 6 views from the popular 'Valbonne church' image set. Some of them are shown on figure 5, together with the 6 input segments and 13 inputs points. The cameras were obtained by Euclidean bundle adjustment over a set of points [11]. The RMS reprojection errors we obtained were:

Algebraic	Poly	Gauss-Newton	3DTriangulation
1.37 pixels	0.77 pixels	0.77 pixels	0.56 pixels

Frame 1 Frame 3 Frame 6

Figure 5: 3 out of the 6 images taken from the 'Valbonne church' sequence, overlaid with 6 matching segments and 13 corresponding points.

Figure 6 (a) shows lines and points reprojected from the 3D reconstruction. The reprojection errors we obtained for the points shown on figure 6 (b) were:

Point	Algebraic	Poly	Gauss-Newton	3DTriangulation
1	4.03 pixels	2.14 pixels	2.14 pixels	1.83 pixels
2	6.97 pixels	1.95 pixels	1.95 pixels	1.52 pixels
3	2.84 pixels	2.21 pixels	2.21 pixels	1.61 pixels
4	4.65 pixels	2.14 pixels	2.14 pixels	1.79 pixels

The reprojection error for 3DTriangulation is slightly lower than for Poly / Gauss-Newton. This indicates that the point on line constraint is feasible on these data.

The 'Building' sequence. This sequence is a continuous video stream consisting of 387 frames, showing a building imaged by a hand-held camera, see figure 7. We reconstructed calibrated cameras by bundle adjustment from interest points that were tracked using a correlation based tracker.

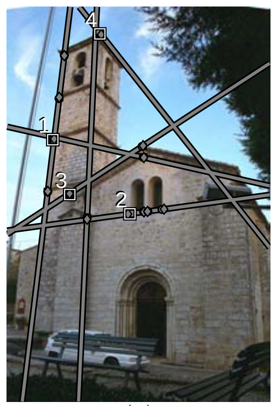

(a)

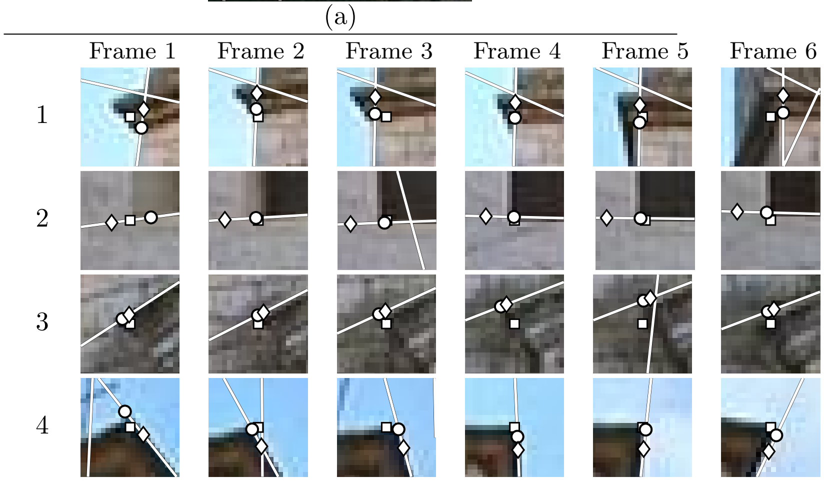

(b)

Figure 6: Reprojected 3D lines and 3D points. (a) shows 4 different numbered points, for which (b) shows a close up for all the 6 images. The squares are the original points, the diamonds are the points reconstructed by ALGEBRAIC, and the circles are the points reconstructed from POLY and GAUSS-NEWTON (they are undistinguishable).

The segment we tracked is almost the only one that is visible throughout the sequence, and thus allows to test our triangulation methods for a very large number of views, namely 387. For the 7 points we selected, we obtained a mean reprojection error of 4.57 pixels for Algebraic, of 3.45 pixels for Poly and Gauss-Newton. Unconstrained triangulation gave a 2.90 pixels reprojection error. These errors which are higher than for the two previous data sets, are explained by the fact that there is non negligible radial distortion in the images, as can be seen on figure 7.

Frame 1

Frame 200

Frame 387

Figure 7: 3 out of the 387 images of the ‘building’ sequence, overlaid with the matching segments and 7 corresponding points.

7 Conclusions

We proposed an algorithm for the optimal triangulation, in the Maximum Likelihood sense, of a point lying on a given 3D line. Several transformations of 3D space and in the images lead to a degree-($3n$-2) polynomial equation. An efficient algorithm computes the real roots leading to feasible points only. Experimental evaluation on simulated and real data show that the method can be applied to large numbers of images, up to 387 in our experiments. The experiments were done for many different real data sets, indoor and outdoor, small, medium and large number of images, calibrated and uncalibrated reconstructions. Comparison of triangulated points with ground truth for the case of simulated data show that using the line constraint greatly improves the accuracy of the reconstruction.

Future work will be devoted to extending the method to the triangulation of points lying on parameterized curves.

Acknowledgements. The first author thanks Frederik Schaffalitzky and Andrew Zisserman for the projection matrices of the 'Valbonne church' sequence.

References

[1] F. S. Acton. *Numerical Methods That Work*. Washington: Mathematical Association of America, 1990. Corrected edition.

[2] A. Bartoli, M. Coquerelle, and P. Sturm. A framework for pencil-of-points structure-from-motion. In *Proceedings of the European Conference on Computer Vision*, 2004.

[3] A. Bartoli and P. Sturm. Multiple-view structure and motion from line correspondences. In *Proceedings of the International Conference on Computer Vision*, 2003.

[4] O. Chum, T. Pajdla, and P. Sturm. The geometric error for homographies. *Computer Vision and Image Understanding*, 97(1):86–102, January 2005.

[5] R. Hartley and F. Schaffalitzky. L_∞ minimization in geometric reconstruction problems. In *Proceedings of the International Conference on Computer Vision and Pattern Recognition*, 2004.

[6] R. Hartley and P. Sturm. Triangulation. *Computer Vision and Image Understanding*, 68(2):146–157, 1997.

[7] R. I. Hartley and A. Zisserman. *Multiple View Geometry in Computer Vision*. Cambridge University Press, 2003. Second Edition.

[8] Q.T. Luong and T. Vieville. Canonic representations for the geometries of multiple projective views. *Computer Vision and Image Understanding*, 64(2):193–229, 1996.

[9] D. Nistèr. *Automatic Dense Reconstruction From Uncalibrated Video Sequences*. PhD thesis, Royal Institute of Technology, KTH, March 2001.

[10] J. Oliensis. Exact two-image structure from motion. IEEE *Transactions on Pattern Analysis and Machine Intelligence*, 24(12):1618–1633, 2002.

[11] F. Schaffalitzky and A. Zisserman. Multi-view matching for unordered image sets. In *Proceedings of the European Conference on Computer Vision*, 2002.

[12] C. Schmid and A. Zisserman. The geometry and matching of lines and curves over multiple views. *International Journal of Computer Vision*, 40(3):199–234, 2000.

[13] H. Stewénius, F. Schaffalitzky, and D. Nistér. How hard is 3-view triangulation really? In *Proceedings of the International Conference on Computer Vision*, 2005.

[14] A. W. K. Tang, T. P. Ng, Y. S. Hung, and C. H. Leung. Projective reconstruction from line correspondences in multiple uncalibrated images. *Pattern Recognition*, 39(5):889–896, May 2006.